Translational Oncology 31 (2023) 101639

Contents lists available at ScienceDirect

Translational Oncology

journal homepage: www.elsevier.com/locate/tranon

Original Research

Breast cancer stem cell-derived extracellular vesicles transfer ARRDC1-AS1 to promote breast carcinogenesis *via* a miR-4731-5p/AKT1 axis-dependent mechanism

Mingzhu Li *, Conglin Lin, Zhibing Cai

Area N4 of Surgical Oncology, Quanzhou First Hospital Affiliated to Fujian Medical University, No. 1028, Anji South Road, Fengze District, Quanzhou, Fujian 362000, China

A R T I C L E I N F O

Keywords:
Breast cancer
ARRDC1-AS1
microRNA-4731-5p
Breast cancer stem cells
Extracellular vesicles
AKT1
Glutamate
Malignant phenotype

A B S T R A C T

Objectives: Deregulation of long non-coding RNAs (lncRNAs) has been frequently reported in breast cancer (BC). This goes to show the importance of understanding its significant contribution towards breast carcinogenesis. In the present study, we clarified a carcinogenic mechanism based on the ARRDC1-AS1 delivered by breast cancer stem cells-derived extracellular vesicles (BCSCs-EVs) in BC.

Methods: The isolated and well characterized BCSCs-EVs were co-cultured with BC cells. The expression of ARRDC1-AS1, miR-4731-5p, and AKT1 was determined in BC cell lines. BC cells were assayed for their viability, invasion, migration and apoptosis *in vitro* by CCK-8, Transwell and flow cytometry, as well as tumor growth *in vivo* after loss- and gain-of function assays. Dual-luciferase reporter gene, RIP and RNA pull-down assays were performed to determine the interactions among ARRDC1-AS1, miR-4731-5p, and AKT1.

Results: Elevation of ARRDC1-AS1 and AKT1 as well as miR-4731-5p downregulation were observed in BC cells. ARRDC1-AS1 was enriched in BCSCs-EVs. Furthermore, EVs containing ARRDC1-AS1 enhanced the BC cell viability, invasion and migration and glutamate concentration. Mechanistically, ARRDC1-AS1 elevated the expression of AKT1 by competitively binding to miR-4731-5p. ARRDC1-AS1-containing EVs were also found to enhance tumor growth *in vivo*.

Conclusion: Collectively, BCSCs-EVs-mediated delivery of ARRDC1-AS1 may promote the malignant phenotypes of BC cells *via* the miR-4731-5p/AKT1 axis.

Introduction

Breast cancer (BC), as one of the most frequently occurring malignancies among females worldwide [1], is the leading cause of mortality related to cancer [2,3]. In recent years, multiple therapies, including surgery, targeted therapy, radiation therapy, and chemotherapy emerged in the treatment of BC [4,5]. It is becoming increasingly evident that, as a sub-type of stem-like cells, breast cancer stem cells (BCSCs) serve as a contributor to aggressiveness, chemoresistance, and tumor relapse of BC [6], suggesting the association of a high proportion of BCSCs with poor outcomes [7,8]. Recently, tumor cell-derived extracellular vesicles (EVs) can transfer molecules to neighboring cells to exert oncogenic properties, representing druggable targets [9]. For example, BCSCs-derived EVs (BCSCs-EVs) contribute to promotion of the metastatic potential of BC cells *via* delivery of miR-197 [10]. In this context, it is of significance to seek EVs-based therapy to treat BC in regulation of malignant phenotypes.

Intriguingly, EVs-mediated delivery of long non-coding RNAs (lncRNAs) affects the biological characteristics of recipient cells, which is emerging as a novel mechanistic insight for carcinogenesis including breast carcinogenesis [11,12]. For instance, lncRNA SNHG16-enriched EVs from BC cells can cause notable elevations in the epithelial-mesenchymal transition (EMT), migratory and invasive capacities of BC cells [13]. Our bioinformatics analysis revealed that ARRDC1-AS1 was enriched in the BCSCs-EVs, though scarcely documented in BC. ARRDC1-AS1 has been reported to exert tumor-promoting effects on the progression of glioma [14]. It is interesting to note that ARRDC1-AS1 is upregulated in BC, serving as a prognostic marker in this malignant disease [15]. In the subsequent bioinformatics analysis, the binding sites were noted between

* Corresponding author.
E-mail address: lmz783399@126.com (M. Li).

https://doi.org/10.1016/j.tranon.2023.101639
Received 2 November 2022; Received in revised form 17 January 2023; Accepted 3 February 2023
Available online 17 February 2023

ARRDC1-AS1 and microRNA (miR)-4731-5p. The association between lncRNAs and miRNAs leads to improved mechanistic understanding and development of possible therapeutic strategies for BC [16]. The down-regulated expression of miR-4731-5p is correlated with a dismal prognosis in BC [17]. miR-4731-5p was predicted to target AKT1 in BC based on the bioinformatics analysis of this study. Evidence has shown that AKT1 inhibition augments the metastatic potential of BC through EGFR-mediated β-catenin nuclear accumulation [18]. Therefore, we proposed a hypothesis in this study that BCSCs-EVs containing ARRDC1-AS1 might exert oncogenic effects on BC cells through a mechanism involving the miR-4731-5p/AKT1 axis.

Materials and methods

Ethical approval

Animal experiments were performed in accordance with *the Guide for the Care and Use of Laboratory animals* published by the National Institutes of Health. Animal experiment protocols were reviewed and granted by the Animal Ethics Committee of Quanzhou First Hospital Affiliated to Fujian Medical University.

Bioinformatic analysis

EV-related lncRNA dataset in the blood of BC was downloaded from the exoRBase database, including 112 normal peripheral blood samples and 140 peripheral blood samples from BC patients. Differentially expressed lncRNAs, with $|\log FC| > 0.5$ and $p < 0.05$ as the threshold, were screened using the R language "limma" package. The lncRNAs were identified using the GTF annotation file of human lncRNA from GENCODE website (v41).

The BC-related mRNA expression datasets (GSE151191 and GSE80754) and BC-related miRNA expression dataset GSE57897 were downloaded from the GEO database. The GSE151191 dataset includes 4 BCSCs samples from primary BC and 4 BCSCs samples from metastatic BC. The GSE80754 dataset includes 3 normal breast tissue samples and 15 BC tissue samples. The GSE57897 dataset includes 31 normal breast tissue samples and 422 BC tissue samples. Differentially expressed miRNAs, with $|\log FC| > 1$ and $p < 0.05$ as the threshold, were obtained using the R language "limma" package. The expression of candidate genes in BC and normal samples from TCGA was analyzed using the ENCORI database, and the miRNAs that lncRNAs bind to were predicted. The target genes of miRNAs were predicted using the ENCORI and miRDB databases. The protein-protein interaction analysis was conducted with the STRING database. Subsequently, the binding sites between lncRNA-miRNA-mRNA were obtained through the starBase database [19].

Cell culture and lentiviral transduction

Human normal breast epithelial cell line MCF-10A and BC cell lines (MCF-7, MDA-MB-453, and SK-BR-3) were purchased from the Cell Resource Center of Shanghai Institute of Biological Sciences (Shanghai, China). MCF-7 and MCF-10A cells were cultured in DMEM containing 10% FBS, SK-BR-3 in McCoy's 5A medium (Gibco) containing 20% FBS and MDA-MB-453 cells in Leibovitz's L-15 medium (Gibco) containing 10% FBS. These cells were all cultured in a 37 °C incubator with 5% CO_2.

Lentiviral vectors containing shRNA (sh)-negative control (NC), lentiviral vectors containing shRNAs targeting ARRDC1-AS1 (sh-ARRDC1-AS1-1/-2/-3), lentiviral vectors containing sh-AKT1-1/-2/-3, inhibitor NC, miR-4731-5p inhibitor, mimic NC, or miR-4731-5p mimic were provided by GeneChem (Shanghai, China). The day before transduction, the cells were seeded in a 6-well plate (1×10^5 cells/well) and cultured in penicillin-streptomycin-free medium. When reaching 70–90% confluence, BC cells were transduced to obtain stably transduced cell line.

Isolation, characterization, and transduction of BCSCs

The BCSC subpopulation ($CD44^+CD24^-$ cells) was detected by anti-CD44-APC, anti-CD24-PE, IgG1-PE, and IgG1-APC (BD). The BC cells in the logarithmic phase were collected in a sterile centrifuge tube containing DMEM-F12 medium, which was incubated with 200 U/mL Liberase Blendzyme 4 (Roche Diagnostics GmbH, Mannheim, Germany) for 12 h to obtain the single cell suspension. The cells were incubated with anti-CD44-APC, anti-CD24-PE, or control antibody at 4 °C for 30 min, and the rinsing cells were added with sorting solution (1 mL sorting solution/10^8 cells). After centrifugation to remove cell supernatant, cells were collected and resuspended in sorting solution (500 μL/10^8 cells). The cells were identified by flow cytometry (FACSAriaII) and the proportion of $CD44^+CD24^-$ cells was analyzed by BD FACS Diva software on flow cytometry.

3D semi solid sphere culture: the 3000 single cells were seeded into serum-free ultra-low adhesion 24-well plate (Corning Incorporated, NY), and each well was added with 1 mL DMEM/F12 supplemented with B27 (1:50, Invitrogen, Carlsbad, CA), 20 ng/mL EGF (PeproTech, Rocky Hill, NJ), 10 ng/mL basic fibroblast growth factor (bFGF) (Invitrogen), 4 μg/mL insulin (Sigma-Aldrich, St. Louis, MO), and 20% methylcellulose (Sigma). After 7 days, cells were collected [20].

BCSCs were cultured in DMEM/F12 (Gibco) medium [21] containing 10 ng/mL bFGF, 20 ng/mL EGF, 2% B27, 5 mg/mL insulin, and 10,000 IU/mL penicillin-streptomycin, followed by incubation in a 37 °C incubator with 5% CO_2. The day before transduction, the cells were seeded in a 6-well plate (1×10^5 cells/well) and incubated with DMEM/F12 medium without penicillin-streptomycin. BCSCs were transduced upon 70–90% cell confluence, and stably transduced BCSCs were obtained.

Extraction of EVs from BCSCs and identification

The transduced BCSCs were seeded into EV-depleted DMEM/F12 containing 10% FBS, and cultured in a 5% CO_2 incubator at 37 °C for 3 days. The cell supernatant was collected and centrifuged at 8000 g for 30 min to remove cell debris. The EVs were extracted using the Hieff™Quick Extravesicle Isolation Kit (41201ES50, Yeasen Company, Shanghai, China). The cell supernatant and EV separation reagent were added to a centrifuge tube (EP tube) at a ratio of 2: 1, and incubated overnight at 4°C. Next, the sample was centrifuged at 10000 × g for 1-2 h at 4 °C, then the supernatant was removed, and the precipitate was collected and purified using the kit [22]. The protein concentration in EVs was measured by a BCA quantitative kit (Beyotime Biotechnology, Jiangsu, China).

The size distribution of EVs was determined using Nanosight nanoparticle tracking analyzer (Malvern Panalytical, Malvern, UK) by nanoparticle tracking analysis (NTA). The expression of surface markers of EVs (CD63, CD81 and TSG101) and non-EVs (Calnexin) was determined using Western blot analysis based on such antibodies as TSG101 (ab30871, Abcam, Cambridge, UK), CD81 (ab92726, Abcam), CD63 (ab134045, Abcam) and Calnexin (ab133615, Abcam). The morphology of EVs was characterized by a transmission electron microscope (TEM) (JEM-1010, JEOL, Tokyo, Japan) [23].

Co-culture of EVs with BC cells

BC cells (5×10^5 cells/well) in the logarithmic growth phase were seeded into a 6-well plate in 5% FBS-containing medium. Subsequently, 20 μg EVs extracted from BCSCs were uniformly mixed with PKH26 (RED, 1: 1000), and incubated at 37 °C for 15 min. Finally, PKH26-labeled EVs were co-cultured with green fluorescent protein (GFP)-labeled BC cells, and then incubated with 200 μL of 1% BSA-containing PBS for 20 min at room temperature. After samples were fixed in VECTASHIELD fixation medium (Vector Labs, Burlingame, CA), the nucleus was stained blue with DAPI. Olympus BX61 confocal fluorescence

microscope (Zeiss Meta 510, Thornwood, NY) was used to observe the uptake of EVs by BC cells.

Fluorescence in situ hybridization (FISH) assay

When reaching 60–70% confluence, BC cells were fixed in 4% formaldehyde, and then permeabilized with 0.5% Triton X-100 in PBS at 4 °C. The cells were incubated with the Cy3-labeled ARRDC1-AS1 probe mixture at 37 °C overnight, and washed 6 times with pre-warmed 2 × saline sodium citrate (SSC) for 3 min each time. Next, the FITC-labeled miR-4731-5p probe was incubated with pre-hybridization buffer (1: 100) using a PCR machine (Bio-Rad, Hercules, CA). The cells were added with FITC-labeled miR-4731-5p probe, and incubated overnight at 37 °C. Next, the cells were stained with DAPI, and photographed under the Leica TCS-SP2 laser scanning confocal microscope.

Assessment of glutamate concentration

BC cells were seeded in a 6-well plate at 2.0×10^5 cells/well and cultured. After 48 h, the concentration of glutamate was measured using the glutamate detection kit (ab83389, Abcam) in the culture medium as previously described [24].

Cell counting (CCK)-8 assay

Cell viability was measured using CCK-8 kit (Dojindo Molecular Technologies, Inc., Kumamoto, Japan) as previously described [25]. BC cells were seeded (1000 cells per well) in a 96-well plate, and added with 100 μL of complete medium, followed by culture for 12, 24, 48, or 72 h. Each well was incubated with 100 μL of RPMI-1640 medium containing 10 μL of CCK-8 for another 3 h culture at 37 °C, with optical density read at 450 nm.

Transwell migration and invasion assays

Cells were seeded in the apical chamber of 24-well Transwell plates (8 μm) in the absence of Matrigel (for migration assay) or pre-coated with Matrigel (for invasion assay) (Corning, New York). BC cells were seeded (10^5 cells/well) in the apical chamber at 37 °C for incubation for 24 h. The cells were fixed with 100% methanol and stained with crystal violet. The stained penetrated cells were photographed with an inverted optical microscope (CarlZeiss, Inc., Oberkochen, Germany), and quantified using Imagine J software [26].

Flow cytometry

Cells were trypsinized (0.25%) in the absence of ethylenediaminetetraacetate (EDTA) and centrifuged, with the supernatant discarded. Based on the manufacturer's protocol of the Alexa Fluor 488 annexin V/PI cell apoptosis kit (Thermo Fisher), the cells were resuspended in 100 μL medium and incubated with 5 μL annexin-V and 1 μL PI at room temperature for 15 min. A BD LSR II flow cytometer (BD Biosciences, Sparks, MD) was used to detect apoptosis [27].

Reverse transcription quantitative polymerase chain reaction (RT-qPCR)

TRIzol-extracted total RNA from tissues or cells was reversely transcribed into complementary (cDNA) using PrimeScript Reverse Transcriptase Kit (Takara, Dalian, China). Reverse transcription and relative quantification of miRNA were determined using TaqMan MicroRNA Reverse Transcription Kit (Thermo Fisher Scientific). As for measurement of the expression of ARRDC1-AS1 in EVs, the synthesized endogenous reference 0.1 ng (1.8×10^8 copies) λpolyA+ RNA (Takara) was added at the beginning of RNA reverse transcription to normalize the total RNA of EVs [28,29]. As normalized to ATCB or U6, the relative expression of genes to be tested was calculated using $2^{-\Delta\Delta Ct}$ method. The primer sequences are listed in Table S1.

Western blot analysis

Total protein in cells and tissues were extracted using RIPA lysis buffer, with concentration measured using the BCA kit. After SDS-PAGE, the isolated protein was transferred to the PVDF membrane and blocked in 5% blotting-grade blocker (Bio-Rad) in TBST for 1 h. The membrane was incubated with the primary antibodies: anti-AKT1 (ab81283, 1: 1000, Cell Signaling Technology, Beverly, MA), anti-AKT (phospho T308, ab38449, 1: 1000, Abcam) and anti-β-actin (#4970, 1: 1000, Abcam; internal reference) overnight at 4 °C, and re-probed with horseradish peroxidase (HRP)-labeled rabbit anti-human IgG (1: 20000, ab205718, Abcam). The blots were visualized using an enhanced chemiluminescence (ECL) kit (Bio-Rad), and quantified by Image Lab analysis software [30].

Dual-luciferase reporter gene assay

The 3'-untranslated region (3'-UTR) binding sites between ARRDC1-AS1 and miR-4731-5p as well as those miR-4731-5p and AKT1 were predicted by the starBase database, and site-directed mutations were performed on the binding sites using the QuikChange site-directed mutagenesis kit (Stratagene, La Jolla, CA). The wild-type (WT) or mutant (MUT) AKT1-3′UTR or ARRDC1-AS1 fragment was inserted into the Pmel and XhoI or Xba1 restriction sites of the pmirGLO luciferase vector (Promega, Madison, WI). The reporter plasmid (0.2 μg) and miRNA mimic or mimic NC (40 nM) were co-transfected using Opti-MEM (Invitrogen) and Lipofectamine 3000 for 48 h, and the luciferase activity was measured using Dual-Luciferase Reporter Assay System (Promega) as normalized to renilla luciferase.

RNA binding protein immunoprecipitation (RIP) and RNA pull-down assay

The binding of ARRDC1-AS1 to AGO2 protein was determined using RIP kit (17-701, Millipore, Billerica, MA) [31]. Cells were lysed in RIPA lysis buffer and centrifuged at 32876.4 g at 4 °C to harvest the supernatant. A part of the cell extract was taken out as Input, and the rest part was incubated for co-precipitation with the antibody rabbit anti-rat AGO2 (1: 100, ab32381, Abcam) or goat anti-rat IgG (1: 100, ab205719, Abcam). The magnetic bead-antibody complex was resuspended in 900 μL RIP Wash Buffer, and incubated with 100 μL cell extract overnight at 4 °C. The magnetic bead-protein complex was collected. The samples and Input were digested with proteinase K and RNA was extracted for subsequent PCR to determine the enrichment of ARRDC1-AS1.

BC cells were transduced with biotin-labeled Bio-NC, Bio-miR-4731-5p-WT and Bio-miR-4731-5p-Mut RNA (50 nM). After transduction for 48 h, the cells were washed with PBS, and incubated with in lysis buffer containing protease inhibitor (Roche) and ribonuclease inhibitor (Fermentas, St. Leon Rot, Germany) on ice for 10 min. The lysate was incubated with streptavidin-coated magnetic beads (M-280, Invitrogen) at 4 °C overnight. The magnetic beads were precoated with RNase free BSA (Sigma) and yeast tRNA (Sigma). The ARRDC1-AS1 enrichment was measured by RT-qPCR.

In vivo tumorigenesis in nude mice

Forty 6-week-old female BALB/c nude mice (Vital River Laboratory Animal Technology Co., Ltd., Beijing, China) were raised at 12/12 h light-dark cycles with humidity of 40–60% at 20–24 °C. The 5×10^6 BC cells in the logarithmic growth phase were dispersed in 100 μL PBS and subcutaneously injected into the right side of the mouse shoulder. Tumor growth was monitored every 5 days throughout the experiment. The experiment was ended on the 35th day, the mice were euthanized by

cervical dislocation. Then the tumor tissues were removed, photographed and the tumor weight was measured. The length and width of the tumor were measured using vernier calipers. The calculation formula for tumor volume was as follows: $0.5*a*b^2$ (a: long axis; b: short axis).

The mouse model of BC was injected into the caudal vein with PBS, EVs, EVs-sh-NC and EVs-sh-ARRDC1-AS1 ($n = 10$) twice a week for 3 weeks. Each injection contained 10 μg EVs or the same amount of PBS.

Ki67 immunohistochemistry

Paraffin sections of tumor tissues were deparaffinized, and incubated with 3% H_2O_2 (diluted in methanol) at room temperature for 10 min. The antigen was retrieved in citrate buffer, and sections were blocked with 5% BSA, followed by incubation with primary antibody rabbit anti-mouse Ki67 (1: 1, ab21700, Abcam) overnight at 4 °C. Afterwards, the sections were reacted with HRP-conjugated secondary antibody anti-rabbit IgG polyclonal goat antibody (1: 500, ab6721, Abcam) at 37 °C for 1 h. The sections were subjected to color development using DAB, counterstained with hematoxylin, and observed under a microscope [32].

TUNEL staining

Sections were treated with 20 μg/mL proteinase K for 20 min at room temperature, and then with 3% H_2O_2 methanol solution for 10 min to block endogenous peroxidase activity. The sections were incubated overnight at 4 °C in a labeling reaction mixture containing terminal deoxynucleotidyl transferase and deoxynucleotides. After incubation, the sections were incubated with horseradish peroxidase (POD, 1: 500) for 30 min at room temperature and treated with DAB solution for 15 min in the dark at room temperature. The sections were counter-stained with hematoxylin, and finally observed under a microscope to observe TUNEL-positive cells with brown-yellow granules in the nuclei [27].

Statistical analysis

Data were summarized as mean ± standard deviation and analyzed by SPSS 21.0 software (IBM Corp., Armonk, NY), with $p < 0.05$ as a level of statistical significance. Unpaired *t* test was used for data comparison between the two groups. One-way analysis of variance (ANOVA) or repeated measures ANOVA combined with Tukey's post hoc test was used to compare data among multiple groups.

Results

ARRDC1-AS1 is highly expressed in BC cells and BCSCs-EVs

BCSCs have the characteristics of chemotherapy resistance, radiotherapy resistance, hypoxia resistance, high tumorigenicity, high invasion, and metastasis [10,33]. These cells play an important role in the tumorigenesis, development, recurrence and metastasis of BC mainly through regulation of the tumor microenvironment (TME) [34]. It is the major way for BCSCs to regulate the TME and promote the malignant progression of tumors by secreting EVs, which carry various components including mRNAs, miRNAs, lncRNAs, DNA, proteins, and lipids to the outside of the cells [35–37].

Accumulating studies have shown that lncRNAs carried by tumor-associated EVs, such as lncRNA HISLA [38], lncRNA HOTAIR [39], lncRNA MALAT1 [40], induce phenotypic changes in TME and tumor cells themselves when delivered to recipient cells by EVs, thereby driving cancer progression [41]. Based on the important role of lncRNAs in EVs, we expect to find EV-delivered lncRNAs from BCSCs that can augment the progression of BC through further research, so as to provide more insights into the mechanism of BCSCs in maintaining malignant phenotypes.

In this study, we first retrieved the exoRBase database and obtained 92 upregulated lncRNAs (≥ 2 folds) in the blood-derived EVs of BC patients (Fig. 1A). In addition, differential analysis of the BCSC-related dataset GSE151191 identified 55 upregulated lncRNAs (≥ 10 folds) (Fig. 1B). The intersection analysis of the lncRNAs from the exoRBase database and the GSE151191 dataset pointed to two candidate lncRNAs (HOTAIRM1 and ARRDC1-AS1) (Fig. 1C). Among them, only ARRDC1-AS1 was significantly highly expressed in BC samples in TCGA database compared to normal samples ($p < 0.001$; Fig. 1D). As shown in Fig. 1E, in the exoRBase database, ARRDC1-AS1 expression was also found to be increased in blood-derived EVs from BC patients ($p < 0.01$). For further validation, RT-qPCR was used to detect ARRDC1-AS1 expression in human normal breast epithelial cells MCF-10A and BC cells MCF-7, MDA-MB-MB-453, and SK-BR-3. The results revealed that higher ARRDC1-AS1 expression was observed in BC cells than that in MCF-10A cells, with MCF-7 cells showing the highest ARRDC1-AS1 expression (Fig. 1F). Thus, ARRDC1-AS1 is highly expressed in BC cells and BCSCs-EVs.

Silencing of ARRDC1-AS1 in BCSCs inhibits the malignant phenotypes of BC cells

Since ARRDC1-AS1 was highly expressed in BCSCs-EVs and BC cells, we moved to elucidate its role in the malignant progression of BC. We selected the MCF-7 cells showing the highest ARRDC1-AS1 expression (Fig. 1F) for cell sorting by flow cytometry. The BCSC $CD44^+CD24^-$ subpopulation was obtained accordingly (Fig. 2A).

After 7 days of 3D semi-solid spheroid culture, sphere growth was observed in BCSCs, which possessed typical characteristics of CSCs (Fig. S1A). Next, EVs were extracted from BCSCs and identified using TEM and NTA. Most EVs were lipid bilayer-enclosed vesicles with a diameter of about 100 nm (Fig. 2B-C). In addition, Western blot analysis displayed that the EVs markers CD63, TSG101, and CD81 were positive, while the non-EVs markers, such as Calnexin, were negative (Fig. 2D). These findings indicated that the BCSCs-EVs were successfully extracted.

The uptake of BCSCs-EVs by BC cells was then observed under the immunofluorescence microscope, which displayed that a large number of BCSCs-EVs entered the BC cells and were distributed around the nuclei (Fig. 2E). Under visual fields, more than 95% cells took up fluorescent EVs. This result ensured that the RNA carried by EVs also entered cells to exert corresponding biological functions.

After confirming that the basic properties and uptake efficiency of BCSCs-EVs met the requirements, we further investigated the effect of ARRDC1-AS1 on the malignant phenotypes of BC cells. First, we designed three shRNA sequences targeting ARRDC1-AS1 (sh-ARRDC1-AS1-1, sh-ARRDC1-AS1-2 and sh-ARRDC1-AS1-3), and verified the silencing efficiency by RT-qPCR. The sh-ARRDC1-AS1-1 exhibiting the best silencing efficiency was selected for the subsequent experiments (Fig. S1B). BCSCs were transduced with sh-ARRDC1-AS1 and RT-qPCR showed that ARRDC1-AS1 expression was reduced in both BCSCs and BCSCs-EVs treated with sh-ARRDC1-AS1 (Fig. 2F). Subsequently, BC cells were co-cultured with EVs or EVs-sh-ARRDC1-AS1 for 24 h. The results of RT-qPCR showed that ARRDC1-AS1 expression was increased (> 2 folds) in BC cells co-cultured with EVs or EVs-sh-NC compared to control BC cells, while it was reduced in BC cells co-cultured with EVs-sh-ARRDC1-AS1 to a level similar to that of the control cells (Fig. 2G).

In addition, CCK-8 assay, Transwell assay, and flow cytometry indicated that BC cell proliferation, migration, and invasion were promoted, and the apoptosis was suppressed (> 60% relative to the control group) upon co-culture with EVs or EVs-sh-NC, while these effects were abolished by EVs-sh-ARRDC1-AS1 (Fig. 2H, I, K, L). These data suggested that ARRDC1-AS1 overexpression could enhance malignant phenotypes of BC cells.

According to a previous report, elevated glutamate levels in the extracellular environment of fast-growing glioblastoma actively kill the surrounding cells and create necessary space for cell invasion [42]. At

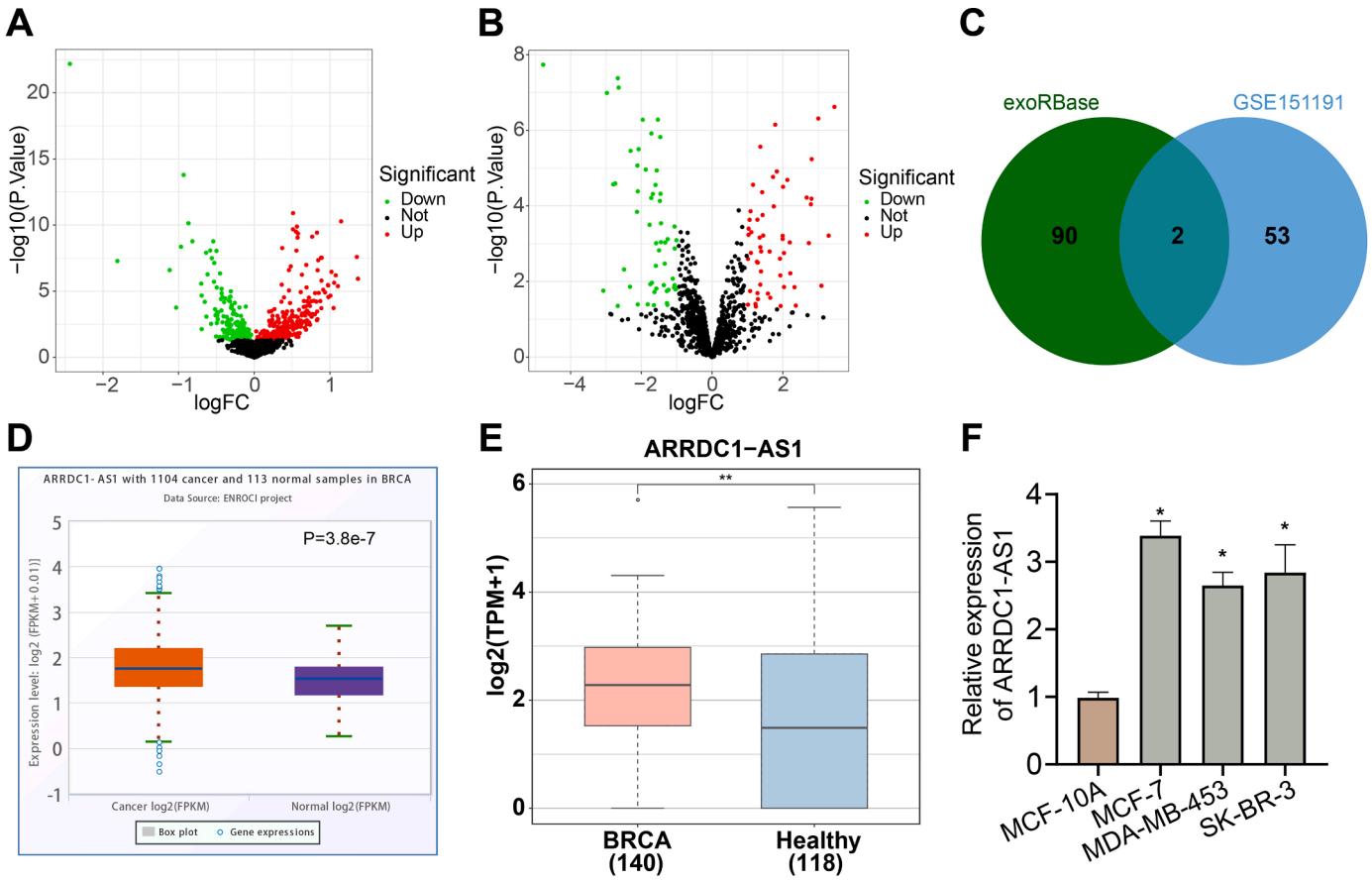

Fig. 1. Differentially expressed lncRNAs in BCSCs-EVs predicted based on bioinformatics analysis. A, A volcano map of differentially expressed lncRNAs in blood-derived EVs of BC patients. B, A volcano map of the differentially expressed lncRNAs in the GSE151191 dataset. C, The intersection of the upregulated lncRNAs in the blood-derived EVs of BC patients and the upregulated lncRNAs in BCSCs. D, ARRDC1-AS1 expression in BC and normal samples in the ENCORI database. E, ARRDC1-AS1 expression in BC and normal samples in the exoRBase database. ** $p < 0.01$ *vs.* normal samples. F, ARRDC1-AS1 expression in human normal breast epithelial cells MCF-10A and BC cells (MCF-7, MDA-MB-MB-453, and SK-BR-3) measured by RT-qPCR. * $p < 0.05$. The cell experiment was repeated three times.

the same time, compared with benign prostatic hyperplasia tissues, the glutamate level is increased in prostate cancer cell lines; the serum glutamate level in most prostate cancer patients is also increased compared with healthy individuals; this increase directly correlates to aggressiveness [43,44]. It can be seen that the level of glutamate is closely related to the change of tumor invasion ability. To this end, we detected the concentration of glutamate in BC cell culture medium by glutamate detection kit. The results demonstrated that glutamate concentration was elevated in the culture medium of BC cells co-cultured with EVs (51%) or EVs-sh-NC (45%) compared to control cells, while silencing of ARRDC1-AS1 decreased the concentration to 25% relative to co-culture with EVs-sh-NC (Fig. 2J). Cumulatively, silencing of ARRDC1-AS1 in BCSCs suppressed malignant phenotypes of BC cells.

ARRDC1-AS1 competitively binds to miR-4731-5p in BC cells

LncRNAs mainly regulate gene expression at the transcriptional level and post-transcriptional level in cells, thereby affecting the growth of tumors. At the post-transcriptional level, lncRNAs sequester miRNAs to release expression of the target genes by competitively binding to miRNA-targeted 3′-UTR or derive mature miRNAs to indirectly regulate the expression of target genes to exert functions [45]. Therefore, we shifted to verify whether ARRDC1-AS1 also promoted the tumor malignant progression through miRNAs. We performed differential expression analysis of miRNA based on the BC-associated miRNA dataset GSE57897 obtained from the GEO database. The results yielded 53 significantly downregulated miRNAs (≥ 10 folds) (Fig. 3A). In addition, the possible miRNAs bound by ARRDC1-AS1 were predicted by the ENCORI database and then intersected with the significantly downregulated miRNAs obtained from the GSE57897 dataset, yielding only one candidate miRNA, namely miR-4731-5p (Fig. 3B).

Subsequently, the possible regulatory effect of ARRDC1-AS1 on miR-4731-5p was explored. RIP assay combined with RT-qPCR showed that the enrichment level of ARRDC1-AS1 was significantly increased by 3.8 folds in the AGO2-pulled down samples (Fig. 3C), confirming the existence of miRNAs that bind to ARRDC1-AS1. Furthermore, RNA pull-down assay results presented that ARRDC1-AS1 enrichment level was 3 folds higher in the Bio-miR-4731-5p-WT group than that in the Bio-probe-NC and Bio-miR-4731-5p-MUT groups (Fig. 3D). Meanwhile, FISH data unveiled that ARRDC1-AS1 and miR-4731-5p were co-localized in BC cells (Fig. 3E). In addition, the starBase database predicted the presence of binding sites of ARRDC1-AS1 and miR-4731-5p (Fig. 3F), which were then mutated using site-directed mutagenesis to obtain ARRDC1-AS1-MUT. Further dual-luciferase reporter gene assay indicated that miR-4731-5p mimic reduced the luciferase activity of ARRDC1-AS1-WT but did not affect that of ARRDC1-AS1-MUT (Fig. 3G). These results showed that ARRDC1-AS1 could serve as a platform for miR-4731-5p binding to AGO2. Finally, we examined the effect of altered ARRDC1-AS1 expression on miR-4731-5p. RT-qPCR validated the overexpression or silencing efficiency of ARRDC1-AS1 (both > 2 folds) (Fig. 3H). Meanwhile, RT-qPCR results showed that miR-4731-5p expression was increased in BC cells treated with sh-ARRDC1-AS1 versus treatment with sh-NC, while it was decreased following oe-ARRDC1-AS1 treatment versus treatment with oe-NC (Fig. 3I). These findings

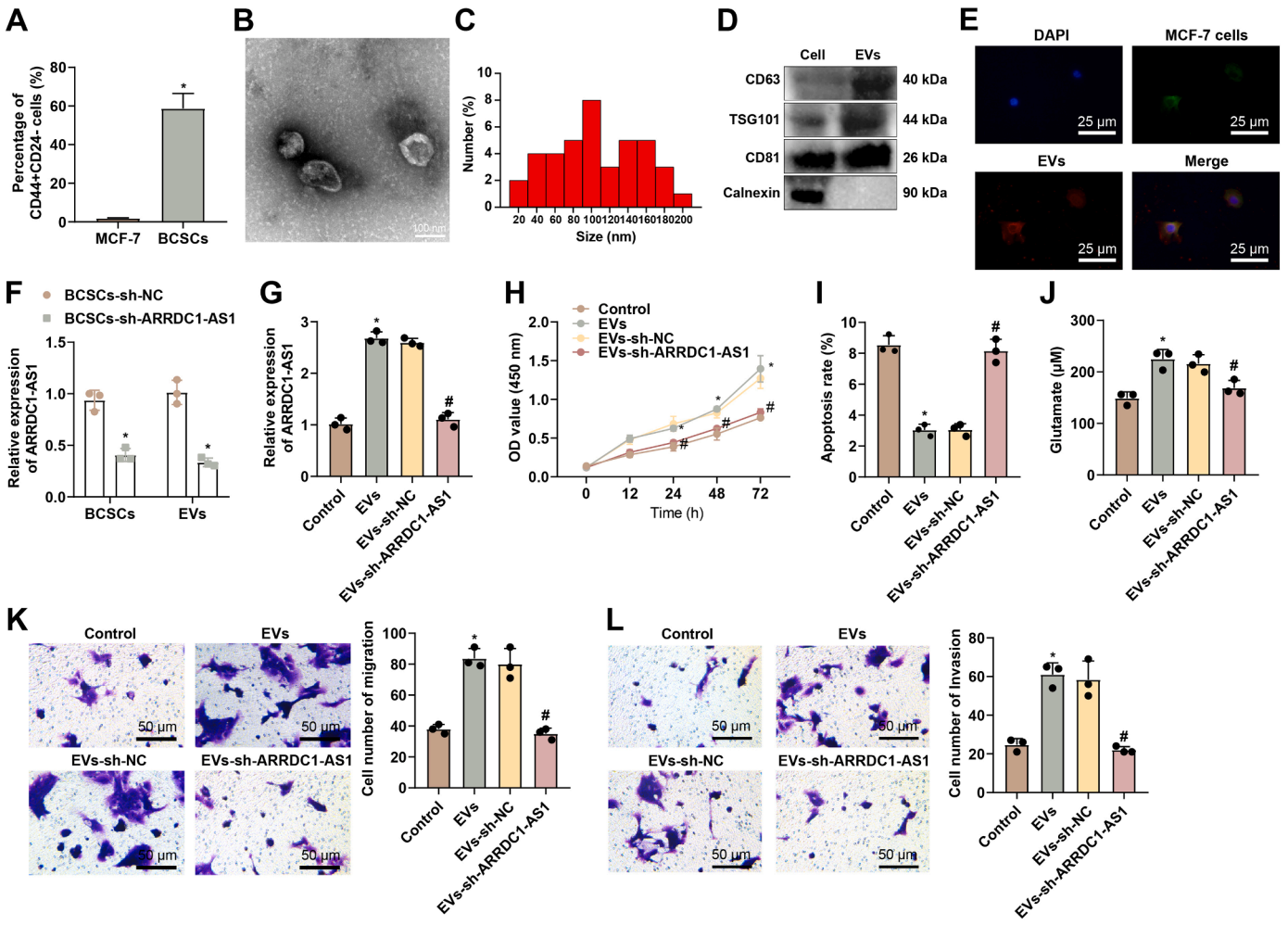

Fig. 2. Effects of BCSCs-EVs containing ARRDC1-AS1 on the malignant phenotypes of BC cells. A, BCSCs isolated from the BC cells by flow cytometry (* $p < 0.05$ *vs.* BC cells). B, The morphology of EVs observed by a TEM. C, Particle size of EVs detected by NTA. D, The expression of CD63, TSG101, CD81, and Calnexin in BCSCs and EVs determined by Western blot analysis. E, The internalization of PKH26-labeled EVs (red) by GFP-labeled BC cells (green) observed under the immunofluorescence microscope. F, ARRDC1-AS1 expression in BCSCs and BCSCs-EVs in the presence of sh-ARRDC1-AS1 determined by RT-qPCR (* $p < 0.05$ *vs.* BCSCs-sh-NC group). G, ARRDC1-AS1 expression in BC cells in the presence of EVs, EVs-sh-NC or EVs-sh-ARRDC1-AS1 measured by RT-qPCR. H, Proliferation of BC cells in the presence of EVs, EVs-sh-NC or EVs-sh-ARRDC1-AS1 detected by CCK-8 assay. I, Apoptosis of BC cells in the presence of EVs, EVs-sh-NC or EVs-sh-ARRDC1-AS1 detected by flow cytometry. J, Glutamate concentration in BC cell culture medium in the presence of EVs, EVs-sh-NC or EVs-sh-ARRDC1-AS1. K, Migration of BC cells in the presence of EVs, EVs-sh-NC or EVs-sh-ARRDC1-AS1 detected by Transwell assay. L, Invasion of BC cells in the presence of EVs, EVs-sh-NC or EVs-sh-ARRDC1-AS1 detected by Transwell assay. In panel G-L, * $p < 0.05$ *vs.* control BC cells; # $p < 0.05$ *vs.* BC cells co-cultured with EVs-sh-NC. The cell experiment was repeated three times.

supported that ARRDC1-AS1 could sponge miR-4731-5p and reduce its expression in BC cells.

miR-4731-5p targets and inhibits AKT1 in BC cells

miR-4731-5p can target mRNAs through complementarity between the miRNA seed sequence (2–8 nt at the 5'UTR) and the target mRNA 3'UTR, which can directly inhibit translation, or cause mRNA instability, thereby degrading the target proteins [46]. Therefore, this study moved to determine the target gene interacting with miR-4731-5p, and to assess whether miR-4731-5p participated in the regulation of BC malignant progression *via* the target gene. Differential analysis of the BC-associated gene dataset GSE80754 was performed, and 845 significantly upregulated genes (≥ 10 folds) were obtained (Fig. 4A). The target genes of miR-4731-5p were predicted by the ENCORI and TargetScan databases, which were intersected with the significantly downregulated genes in the GSE80754 dataset. And 110 candidate target genes were obtained (Fig. 4B). Then, protein-protein interaction analysis indicated that AKT1 was identified as the core protein in the interaction network (Fig. 4C). Therefore, AKT1 was selected for further study.

Next, to explore whether miR-4731-5p could target AKT1. Based on the binding site between miR-4731-5p and AKT1 3'UTR (Fig. 4D), and dual-luciferase reporter gene assay further validated that the luciferase activity of AKT1-WT was suppressed by miR-4731-1-5p mimic (Fig. 4E).

Besides, Western blot analysis suggested that overexpression of ARRDC1-AS1 elevated total AKT1 protein level and the extent of AKT1 phosphorylation, while overexpression of miR-4731-5p caused opposite results. In addition, concomitant increase of ARRDC1-AS1 and miR-4731-5p reduced total AKT1 protein level and the extent of AKT1 phosphorylation, which were close to the control group (Fig. 4F). Therefore, AKT1 was a target gene of miR-4731-5p.

BCSCs-EVs promote the malignant phenotypes of BC cells via ARRDC1-AS1/miR-4731-5p/AKT1

The aforementioned results clarified the downstream targets of ARRDC1-AS1 and miR-4731-5p, and formed a ceRNA regulatory

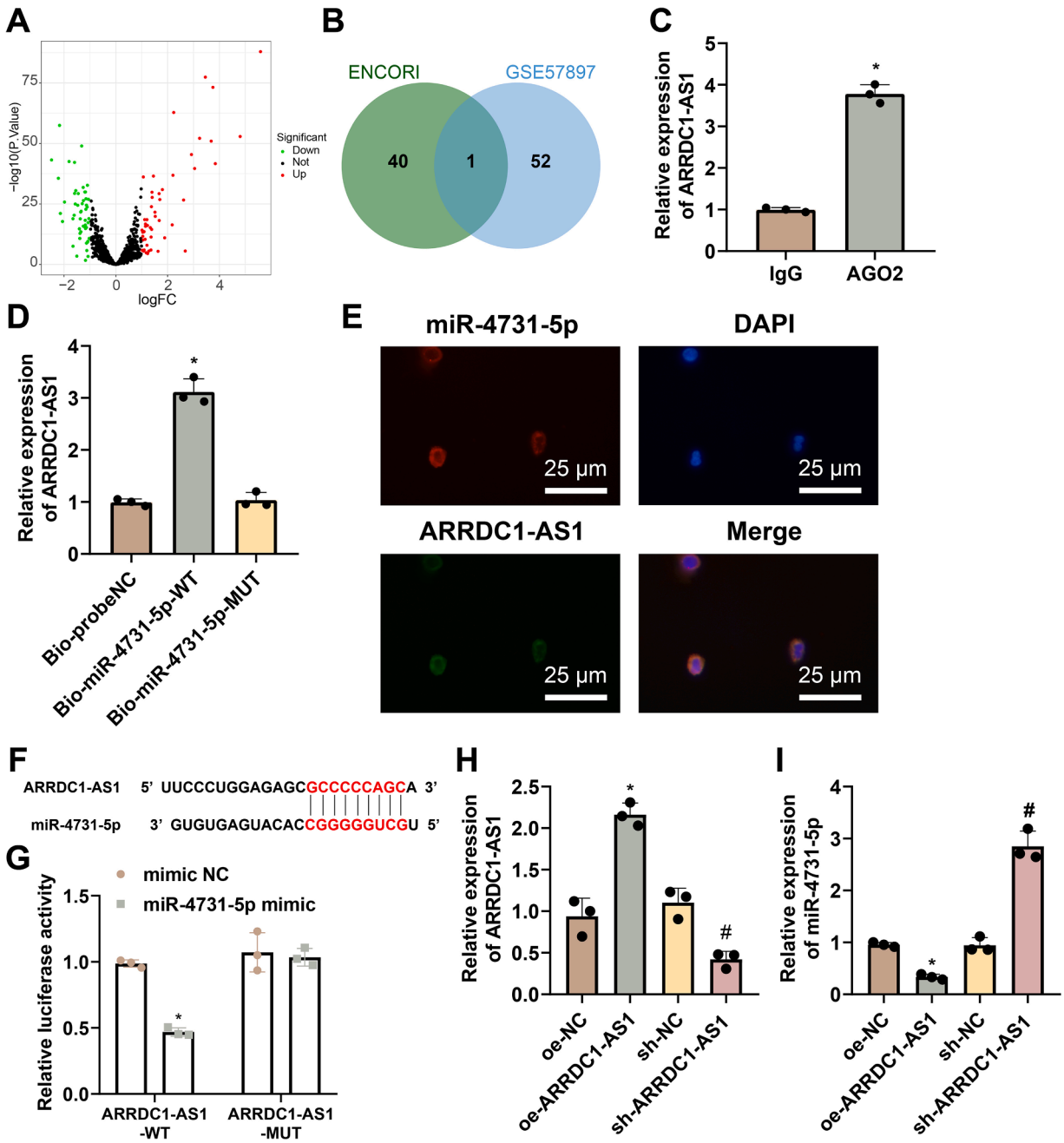

Fig. 3. Binding relationship between ARRDC1-AS1 and miR-4731-5p in BC cells. A, A volcano map of differentially expressed miRNAs in BC-related dataset GSE57897. B, The intersection between miRNA bound by ARRDC1-AS1 and significantly downregulated miRNAs in GSE57897. C, The interaction between miR-4731-5p and ARRDC1-AS1 detected by RIP assay and RT-qPCR (* $p < 0.05$ *vs.* the IgG group). D, The interaction between miR-4731-5p and ARRDC1-AS1 detected by RNA pull-down assay (* $p < 0.05$ *vs.* the Bio-probe NC or Bio-miR-4731-5p-MUT group). E, The co-localization of Cy3-miR-4731-5p (red) and FITC-ARRDC1-AS1 (green) in BC cells detected by FISH assay. F, Binding sites between ARRDC1-AS1 and miR-4731-5p predicted by the starBase database. G, The regulatory effect of ARRDC1-AS1 on miR-4731-5p verified by dual-luciferase reporter gene assay (* $p < 0.05$ the mimic NC group). H, ARRDC1-AS1 expression in BC cells treated with oe-ARRDC1-AS1 or sh-ARRDC1-AS1 determined by RT-qPCR (* $p < 0.05$ *vs.* BC cells transduced with oe-NC; # $p < 0.05$ *vs.* BC cells transduced with sh-NC). I, miR-4731-5p expression in BC cells treated with oe-ARRDC1-AS1 or sh-ARRDC1-AS1 determined by RT-qPCR (* $p < 0.05$ *vs.* BC cells transduced with oe-NC; # $p < 0.05$ *vs.* BC cells transduced with sh-NC). The cell experiment was repeated three times.

network of ARRDC1-AS1/miR-4731-5p/AKT1. Then whether BCSCs-EVs affected the malignant biological behaviors of BC cells by regulating the ceRNA network was the next focus of this study. We co-cultured BCSCs-EVs with BC cells, and selected the sh-AKT1-2 sequence with a superior silencing efficiency (Fig. S1C) to knock down the downstream target gene AKT1. It was found that the expression of ARRDC1-AS1 and AKT1 was increased (2.5 folds), and miR-4731-5p expression was decreased (62%) in BC cells co-cultured with sh-NC + EVs versus co-culture with sh-NC, while further sh-AKT1 treatment reduced AKT1 expression while exerted no effects on the expression of ARRDC1-AS1 and miR-4731-5p. In the presence of sh-AKT1 + EVs, the expression of ARRDC1-AS1 and miR-4731-5p displayed no significant difference, and AKT1 expression was lower in BC cells relative to treatment with sh-NC + EVs (Fig. 5A and B). The above results suggest that ARRDC1-AS1 carried by EVs antagonized the effect of AKT1 silencing to a certain extent through inhibition of miR-4731-5p.

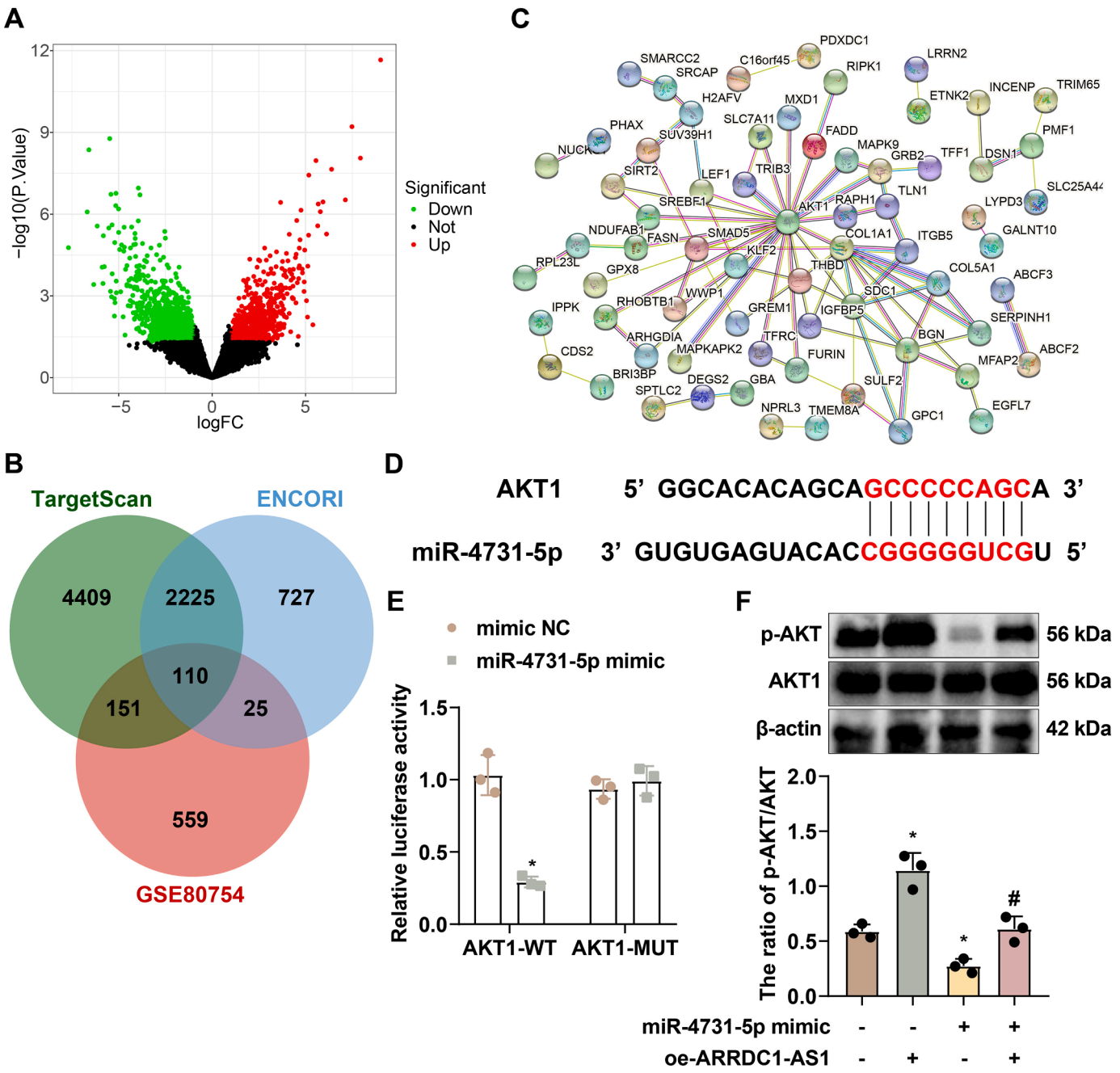

Fig. 4. Binding relationship between miR-4731-5p and AKT1 in BC cells. A, A volcano map of differentially expressed genes in the GSE80754 dataset. B, Intersection between target genes of miR-4731-5p and significantly upregulated genes in the GSE80754 dataset. C, Protein interaction network of the STRING database. D, The binding site between miR-4731-5p and AKT1 predicted by the ENCORI database. E, The binding of miR-4731-5p to AKT1 verified by dual-luciferase reporter gene assay (* $p < 0.05$ *vs.* the mimic NC group). F, Total AKT1 protein level and the extent of AKT1 phosphorylation in BC cells transduced with oe-ARRDC1-AS1 and/or miR-4731-5p mimic measured by Western blot analysis (* $p < 0.05$ *vs.* control BC cells; # $p < 0.05$ *vs.* BC cells transduced with oe-ARRDC1-AS1). The cell experiment was repeated three times.

In addition, based on the results of CCK-8 assay, Transwell assay, and flow cytometry, co-culture with sh-NC + EVs enhanced BC cell proliferation, migration, and invasion, and suppressed apoptosis versus co-culture with sh-NC, while these effects were abolished by sh-AKT1; however, sh-AKT1 + EVs attenuated the inhibiting effect of sh-AKT1 on BC cell proliferation, migration, and invasion, and the promoting effect on cell apoptosis (Fig. 5C, D, F, G). Glutamate concentration in BC cell culture medium was increased after co-culture with sh-NC + EVs compared to co-culture with sh-NC, while silencing of AKT1 decreased glutamate concentration. Combined treatment with EVs and sh-AKT1 led to a 1.9-fold increase of glutamate concentration relative to treatment with sh-AKT1 (Fig. 5E). Overall, these findings indicated that BCSCs-EVs could regulate ARRDC1-AS1/miR-4731-5p/AKT1 to promote the malignant phenotypes of BC cells.

BCSCs-EVs promote the tumorigenesis of BC cells in nude mice by delivering ARRDC1-AS1

Through the above experiments, we confirmed that the ceRNA network of ARRDC1-AS1/miR-4731-5p/AKT1 could maintain the malignant phenotypes of BC cells *in vitro*. In this experiment, we centered on verifying whether the BCSCs-EVs could deliver ARRDC1-AS1 to affect

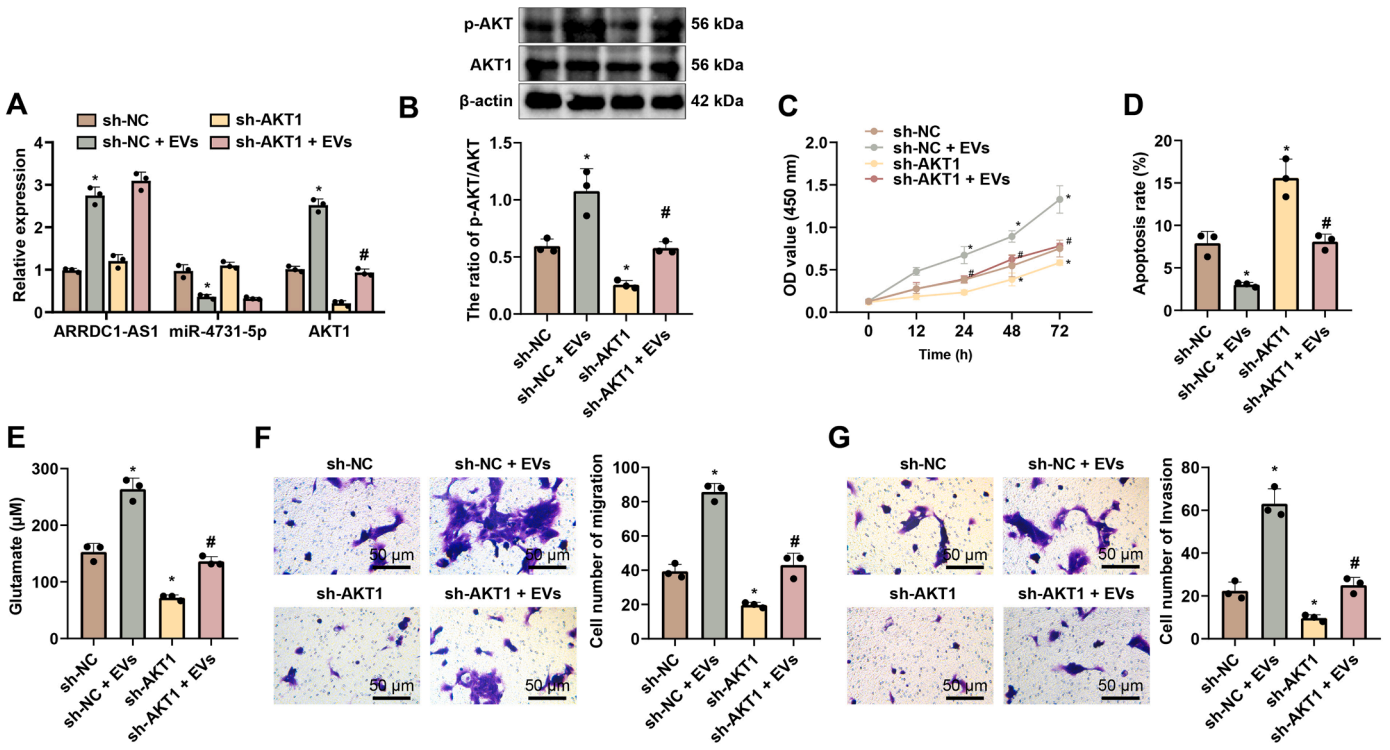

Fig. 5. BCSCs-EVs augment the malignant phenotypes of BC cells *via* regulation of the ARRDC1-AS1/miR-4731-5p/AKT1 axis. BC cells were co-cultured with EVs and/or transduced with sh-AKT1. A, Expression of ARRDC1-AS1, miR-4731-5p, and AKT1 in BC cells measured by RT-qPCR. B, AKT1 protein level in BC cells measured by Western blot analysis. C, Glutamate concentration in BC cell culture medium. D, Proliferation of BC cells detected by CCK-8 assay. E, Migration of BC cells detected by Transwell assay. F, Invasion of BC cells detected by Transwell assay. G, Apoptosis of BC cells detected by flow cytometry. * $p < 0.05$ *vs*. BC cells transduced with sh-NC; # $p < 0.05$ *vs*. BC cells transduced with sh-NC and co-cultured with EVs. The cell experiment was repeated three times.

the growth of BC cells in nude mice. BC nude mouse models were constructed and then injected with EVs, EVs-sh-NC, or EVs-sh-ARRDC1-AS1. It was found that the expression of ARRDC1-AS1 and AKT1 was increased by 2 folds, but miR-4731-5p expression was decreased by 76% in the tumor tissues of mice injected with EVs relative to control mice. Conversely, compared to injection with EVs-sh-NC, injection with EVs-sh-ARRDC1-AS1 reduced the expression of ARRDC1-AS1 and AKT1 to a level similar to that of the control mice and elevated miR-4731-5p expression in the tumor tissues of mice (Fig. 6A-B).

In addition, an increase was noted in the tumor volume and weight of mice injected with EVs relative to control mice; opposite results were found following EVs-sh-ARRDC1-AS1 treatment versus EVs-sh-NC treatment (Fig. 6C–E). Based on the results of TUNEL staining and Ki67 immunohistochemical staining, in the presence of EVs, cell proliferation in the tumor tissue of mice was promoted as shown by 57% increase in the number of Ki67-positive cells and suppressed apoptosis as shown by a nearly 4-fold decline in the TUNEL-positive cells compared to no treatment. However, EVs-sh-ARRDC1-AS1 led to opposite results (Ki67-positive cells decreased by 33% and TUNEL-positive cells increased by 2.8 folds) versus EVs-sh-NC treatment (Fig. 6F–G). Thus, it can be concluded that ARRDC1-AS1 shuttled by BCSCs-EVs induced the tumorigenesis of BC cells in nude mice. It is also further suggested that ARRDC1-AS1 plays an important role in maintaining the stemness of BC cells.

Discussion

BCSCs contribute to the progression, recurrence, metastasis, and chemoresistance of BC [47]. The epigenetics field holds the potential for the development of new BC treatment therapies [48,49], and the evidence obtained in this study suggested that BCSCs-EVs containing ARRDC1-AS1 upregulate the expression of AKT1 by competitively binding to miR-4731-5p, which contributes to malignant progression of BC cells.

EVs shuttle various cellular-derived molecules, including lipids, proteins, DNA, mRNAs, miRNAs, and lncRNAs, to affect BC progression [50]. Cancer-secreted EVs can carry various molecules to target cells to promote multiple aspects of tumor progression [20,21]. For instance, the role of lncRNA NEAT1 as oncogene has been established with evidence indicating that NEAT1 shuttled by BC-secreted EVs could sequester miR-141-3p away from the expression of KLF12, thus driving oncogenic activities and chemo-resistance in BC [51]. Our findings are encouraging and concur with this prior study, showing that lncRNA ARRDC1-AS1 was enriched in BCSCs-EVs. Furthermore, we demonstrated that elevation of ARRDC1-AS1 occurred in the BC cells, and EVs containing ARRDC1-AS1 augmented malignant progression of BC cells, accompanied by increased glutamate concentration. The tumor-promoting role of ARRDC1-AS1 has also been proposed in the context of colon cancer [23]. Although ARRDC1-AS1 has been proposed as a prognostic biomarker in BC, the mechanistic basis remain largely unknown [11]. Moreover, glutamine, the most abundant type of amino acid in human blood circulation, is increased in cancer cells [24]. More specifically, increased concentration of glutamate can induce aggressive BC cells [25]. Therefore, the ARRDC1-AS1-driven increase in glutamate concentration may result in malignant progression of BC. Concordantly, the *in vivo* experiment in our study demonstrated that BCSCs-EVs containing ARRDC1-AS1 promoted the growth of BC in mice. However, the specific mechanisms of ARRDC1-AS1 in BC remain to be further elucidated.

As previously demonstrated, ARRDC1-AS1 activated by STAT1 exerts oncogenic effects by sponging miR-432-5p and elevating PRMT5 expression in glioma [10]. Another important finding in our study was that ARRDC1-AS1 could act a sponge of miR-4731-5p and subsequently upregulated AKT1 expression. We also found that the tumor-inhibiting

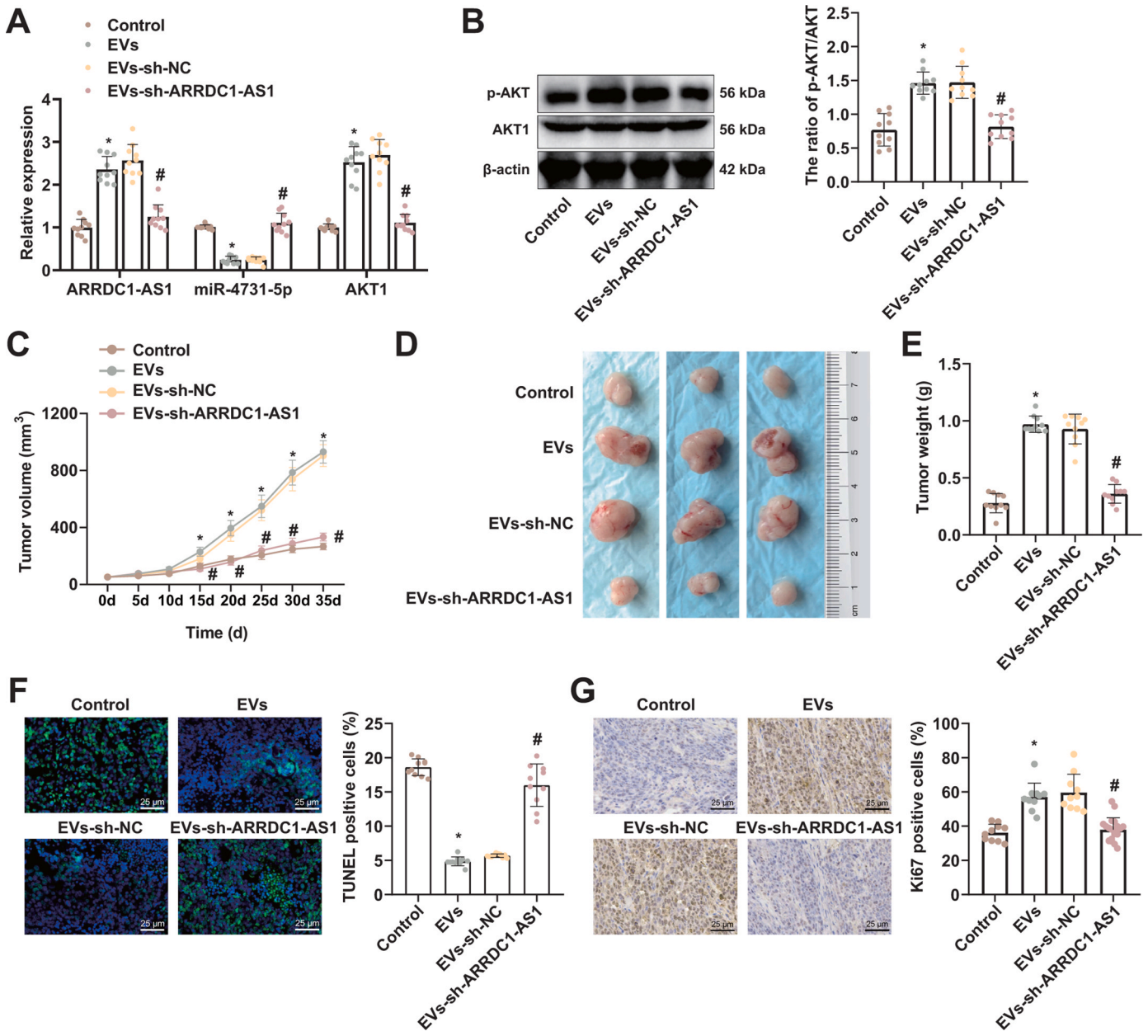

Fig. 6. Effects of BCSCs-EVs delivering ARRDC1-AS1 on the growth of BC cells in nude mice. BC nude mice were injected with EVs, EVs-sh-NC, or EVs-sh-ARRDC1-AS1 ($n = 10$). A, Expression of ARRDC1-AS1, miR-4731-5p and AKT1 in tumor tissues of BC nude mice determined by RT-qPCR. B, AKT1 protein level in the tumor tissues of BC nude mice measured by Western blot analysis. C, Tumor growth of BC nude mice. D, Representative images showing xenografts in BC nude mice. E, Tumor weight of BC nude mice. F, Apoptosis in tumor tissues of BC nude mice detected by TUNEL staining. G, Proliferation of cells in tumor tissues of BC nude mice detected by Ki67 immunohistochemical staining. * $p < 0.05$ *vs.* control mice; # $p < 0.05$ *vs.* mice injected with EVs-sh-NC.

role of miR-4731-5p in BC cells. Downregulation of miR-4731-5p occurs in BC tissues and cells, and upregulated miR-4731-5p suppresses oncogenic behaviors of BC cells by regulating PAICS-dependent phosphorylation of FAK [14]. Meanwhile, lncRNA TMPO-AS1 can sequester miR-4731-5p to release FOXM1 expression, thus leading to BC growth [13]. In the subsequent analysis, miR-4731-5p was confirmed to target AKT1 and negatively modulate the expression of AKT1 in BC. Silencing of AKT1 repressed the malignant phenotypes of BC cells, and increased the glutamate concentration. AKT1, as a member of the serine-threonine kinase class, is implicated in tumor cell processes, including growth and proliferation [15]. Another study has also revealed elevated AKT1 in breast tumors, and that activation of AKT contributes to promoted cell survival and proliferative ability [26], suggesting that overexpressed AKT1 could enhance the malignant behaviors of BC cells. Both *in vitro* and *in vivo* experiments in the present study have validated that ARRDC1-AS1 shuttled by EVs from BCSCs inhibited miR-4731-5p and promoted AKT1 to induce the malignant features of BC, leading to induction of BC growth and tumorigenesis.

Conclusion

The current study sheds new light on the mechanistic actions of ARRDC1-AS1 underlying the malignant phenotypes of BC cells. ARRDC1-AS1, which was enriched in BCSCs-EVs, upregulated the expression of AKT1 by competitively binding to miR-4731-5p to augment the malignant phenotypes of BC cells (Fig. 7). Notably, our findings on the pro-tumorigenic action of ARRDC1-AS1 provide new insights into the mechanism of BC and offer potential targets for

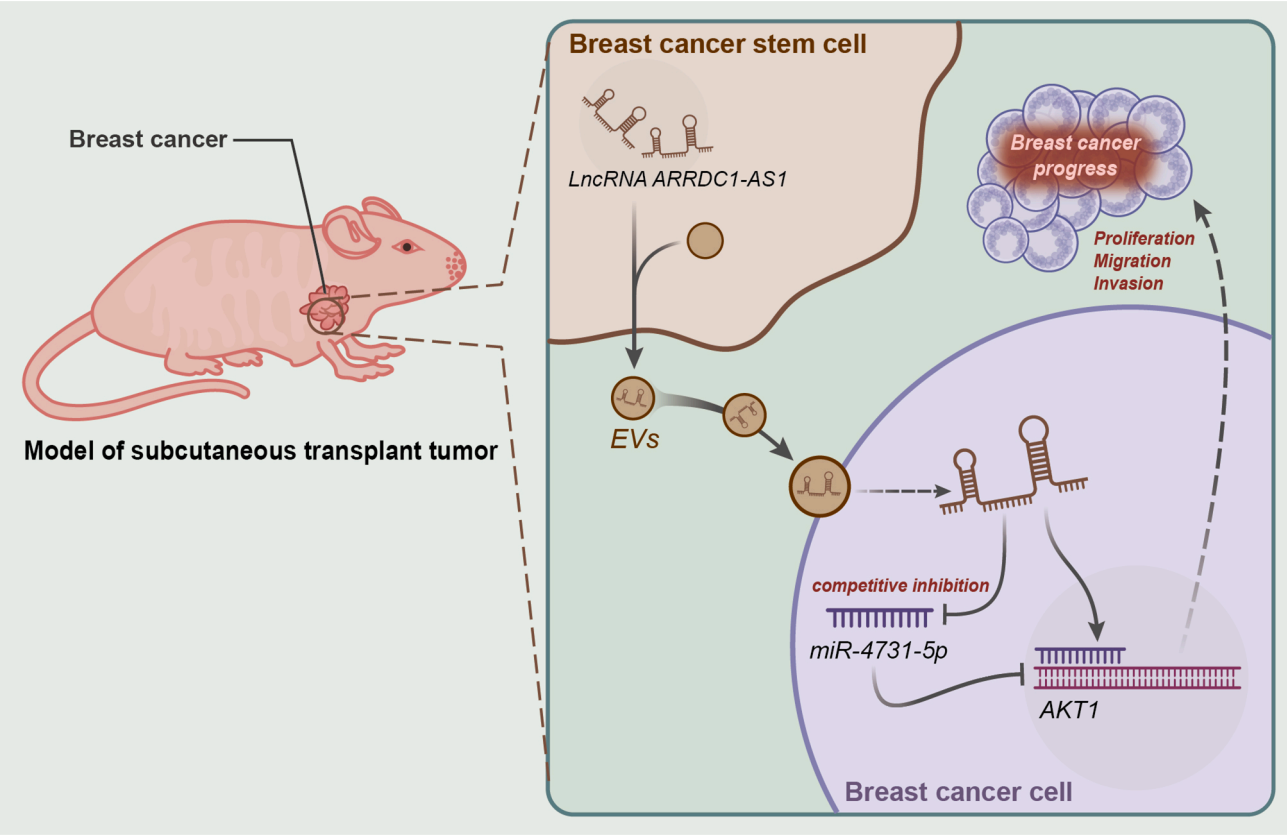

Fig. 7. Molecular mechanisms of the BCSCs-EVs containing ARRDC1-AS1 involved in BC. BCSCs-EVs containing ARRDC1-AS1 upregulate the expression of AKT1 by competitively binding to miR-4731-5p, thereby promoting the proliferation, migration, and invasion of BC cells.

translational applications. However, only a single dose of EVs was adopted in the present study. Identification of the optimum dose and the times of injection would be aimed at in future studies.

Availability of data and materials

The data that supports the findings of this study are available on request from the corresponding author.

Ethics approval and consent to participate

Animal experiments were performed in accordance with *the Guide for the Care and Use of Laboratory animals* published by the National Institutes of Health. Animal experiment protocols were reviewed and granted by the Animal Ethics Committee of Quanzhou First Hospital Affiliated to Fujian Medical University.

Consent for publication

Consent for publication was obtained from the participants.

CRediT authorship contribution statement

Mingzhu Li: Writing – original draft, Conceptualization, Methodology, Formal analysis, Project administration. **Conglin Lin:** Writing – original draft, Conceptualization, Methodology, Formal analysis. **Zhibing Cai:** Writing – original draft, Conceptualization, Methodology, Project administration.

Declaration of Competing Interest

The authors declare that they have no known competing financial interests or personal relationships that could have appeared to influence the work reported in this paper.

Funding

This study was funded by Science and Technology Bureau of Quanzhou City, Fujian Province (2019N038S).

Acknowledgments

Not applicable.

Supplementary materials

Supplementary material associated with this article can be found, in the online version, at doi:10.1016/j.tranon.2023.101639.

References

[1] N. Harbeck, M. Gnant, Breast cancer, Lancet 389 (10074) (2017) 1134–1150.
[2] Y. Liang, H. Zhang, X. Song, Q. Yang, Metastatic heterogeneity of breast cancer: molecular mechanism and potential therapeutic targets, Semin. Cancer Biol. 60 (2020) 14–27.
[3] K.P. Trayes, S.E.H. Cokenakes, Breast cancer treatment, Am. Fam. Phys. 104 (2) (2021) 171–178.
[4] E.S. McDonald, A.S. Clark, J. Tchou, P. Zhang, G.M. Freedman, Clinical diagnosis and management of breast cancer, J. Nucl. Med. 57 (Suppl 1) (2016) 9S–16S.
[5] T. Shien, H. Iwata, Adjuvant and neoadjuvant therapy for breast cancer, Jpn. J. Clin. Oncol. 50 (3) (2020) 225–229.
[6] X. Zeng, C. Liu, J. Yao, H. Wan, G. Wan, Y. Li, et al., Breast cancer stem cells, heterogeneity, targeting therapies and therapeutic implications, Pharmacol. Res. 163 (2021), 105320.
[7] K. Barzaman, J. Karami, Z. Zarei, A. Hosseinzadeh, M.H. Kazemi, S. Moradi-Kalbolandi, et al., Breast cancer: Biology, biomarkers, and treatments, Int. Immunopharmacol. 84 (2020), 106535.

[8] S. Palomeras, S. Ruiz-Martinez, T. Puig, Targeting breast cancer stem cells to overcome treatment resistance, Molecules 23 (9) (2018).
[9] C. Lu, Y. Zhao, J. Wang, W. Shi, F. Dong, Y. Xin, et al., Breast cancer cell-derived extracellular vesicles transfer miR-182-5p and promote breast carcinogenesis via the CMTM7/EGFR/AKT axis, Mol. Med. 27 (1) (2021) 78.
[10] L. Li, Y. Xiong, N. Wang, M. Zhu, Y. Gu, Breast cancer stem cells-derived extracellular vesicles affect pparg expression by delivering microRNA-197 in breast cancer cells, Clin. Breast Cancer 22 (5) (2022) 478–490.
[11] J.J. Qiu, Y.Y. Lin, X.Y. Tang, Y. Ding, X.F. Yi, K.Q. Hua, Extracellular vesicle-mediated transfer of the lncRNA-TC0101441 promotes endometriosis migration/invasion, Exp. Cell Res. 388 (1) (2020), 111815.
[12] Y. Li, Z. Zhao, W. Liu, X. Li, SNHG3 functions as miRNA sponge to promote breast cancer cells growth through the metabolic reprogramming, Appl. Biochem. Biotechnol. 191 (3) (2020) 1084–1099.
[13] W. Xia, Y. Liu, T. Cheng, T. Xu, M. Dong, X. Hu, Extracellular vesicles carry lncRNA SNHG16 to promote metastasis of breast cancer cells via the miR-892b/PPAPDC1A Axis, Front. Cell Dev. Biol. 9 (2021), 628573.
[14] X.D. Zou, Q. Zang, Z.Z. Zhang, Y.Q. Lu, X. Jin, Y. Wu, Long noncoding RNA ARRDC1-AS1 is activated by STAT1 and exerts oncogenic properties by sponging miR-432-5p/PRMT5 axis in glioma, Biochem. Biophys. Res. Commun. 534 (2021) 511–518.
[15] H. Liu, J. Li, P. Koirala, X. Ding, B. Chen, Y. Wang, et al., Long non-coding RNAs as prognostic markers in human breast cancer, Oncotarget 7 (15) (2016) 20584–20596.
[16] Y. Wang, J. Ma, R. Li, X. Gao, H. Wang, G. Jiang, LncRNA TMPO-AS1 serves as a sponge for miR-4731-5p modulating breast cancer progression through FOXM1, Am. J. Transl. Res. 13 (10) (2021) 11094–11106.
[17] L. Lang, J. Tao, C. Yang, W. Li, Tumor suppressive role of microRNA-4731-5p in breast cancer through reduction of PAICS-induced FAK phosphorylation, Cell Death Discov. 8 (1) (2022) 154.
[18] W. Li, J.Z. Hou, J. Niu, Z.Q. Xi, C. Ma, H. Sun, et al., Akt1 inhibition promotes breast cancer metastasis through EGFR-mediated beta-catenin nuclear accumulation, Cell Commun. Signal. 16 (1) (2018) 82.
[19] M.E. Ritchie, B. Phipson, D. Wu, Y. Hu, C.W. Law, W. Shi, et al., limma powers differential expression analyses for RNA-sequencing and microarray studies, Nucleic Acids Res. 43 (7) (2015) e47.
[20] Y.H. Cho, E.J. Ro, J.S. Yoon, T. Mizutani, D.W. Kang, J.C. Park, et al., 5-FU promotes stemness of colorectal cancer via p53-mediated WNT/beta-catenin pathway activation, Nat. Commun. 11 (1) (2020) 5321.
[21] X. Lin, W. Chen, F. Wei, X. Xie, TV-circRGPD6 nanoparticle suppresses breast cancer stem cell-mediated metastasis via the miR-26b/YAF2 Axis, Mol. Ther. 29 (1) (2021) 244–262.
[22] F. Wei, C. Ma, T. Zhou, X. Dong, Q. Luo, L. Geng, et al., Exosomes derived from gemcitabine-resistant cells transfer malignant phenotypic traits via delivery of miRNA-222-3p, Mol. Cancer 16 (1) (2017) 132.
[23] Z. Liao, R. Luo, G. Li, Y. Song, S. Zhan, K. Zhao, et al., Exosomes from mesenchymal stem cells modulate endoplasmic reticulum stress to protect against nucleus pulposus cell death and ameliorate intervertebral disc degeneration *in vivo*, Theranostics 9 (14) (2019) 4084–4100.
[24] Y. Long, H. Tao, A. Karachi, A.J. Grippin, L. Jin, Y.E. Chang, et al., Dysregulation of glutamate transport enhances treg function that promotes VEGF blockade resistance in glioblastoma, Cancer Res. 80 (3) (2020) 499–509.
[25] M.L. Ji, H. Jiang, X.J. Zhang, P.L. Shi, C. Li, H. Wu, et al., Preclinical development of a microRNA-based therapy for intervertebral disc degeneration, Nat. Commun. 9 (1) (2018) 5051.
[26] L. Wang, H. Long, Q. Zheng, X. Bo, X. Xiao, B. Li, Circular RNA circRHOT1 promotes hepatocellular carcinoma progression by initiation of NR2F6 expression, Mol. Cancer 18 (1) (2019) 119.
[27] W. Pan, L. Wang, X.F. Zhang, H. Zhang, J. Zhang, G. Wang, et al., Hypoxia-induced microRNA-191 contributes to hepatic ischemia/reperfusion injury through the ZONAB/Cyclin D1 axis, Cell Death Differ. 26 (2) (2019) 291–305.
[28] L.Y. Lin, L. Yang, Q. Zeng, L. Wang, M.L. Chen, Z.H. Zhao, et al., Tumor-originated exosomal lncUEGC1 as a circulating biomarker for early-stage gastric cancer, Mol. Cancer 17 (1) (2018) 84.
[29] W. Zhao, P. Qin, D. Zhang, X. Cui, J. Gao, Z. Yu, et al., Long non-coding RNA PVT1 encapsulated in bone marrow mesenchymal stem cell-derived exosomes promotes osteosarcoma growth and metastasis by stabilizing ERG and sponging miR-183-5p, Aging 11 (21) (2019) 9581–9596 (Albany NY).
[30] J. Song, W. Zhang, J. Wang, H. Yang, Q. Zhou, H. Wang, et al., Inhibition of FOXO3a/BIM signaling pathway contributes to the protective effect of salvianolic acid A against cerebral ischemia/reperfusion injury, Acta Pharm. Sin. B 9 (3) (2019) 505–515.
[31] D. Yang, J. Qiao, G. Wang, Y. Lan, G. Li, X. Guo, et al., N6-Methyladenosine modification of lincRNA 1281 is critically required for mESC differentiation potential, Nucleic Acids Res. 46 (8) (2018) 3906–3920.
[32] T. Fang, H. Lv, G. Lv, T. Li, C. Wang, Q. Han, et al., Tumor-derived exosomal miR-1247-3p induces cancer-associated fibroblast activation to foster lung metastasis of liver cancer, Nat. Commun. 9 (1) (2018) 191.
[33] D. Liu, Q. Lu, X. Wang, J. Wang, N. Lu, Z. Jiang, et al., LSECtin on tumor-associated macrophages enhances breast cancer stemness via interaction with its receptor BTN3A3, Cell Res. 29 (5) (2019) 365–378.
[34] J.A. Clara, C. Monge, Y. Yang, N. Takebe, Targeting signalling pathways and the immune microenvironment of cancer stem cells - a clinical update, Nat. Rev. Clin. Oncol. 17 (4) (2020) 204–232.
[35] K. Takahashi, I.K. Yan, J. Wood, H. Haga, T. Patel, Involvement of extracellular vesicle long noncoding RNA (linc-VLDLR) in tumor cell responses to chemotherapy, Mol. Cancer Res. 12 (10) (2014) 1377–1387.
[36] Y. Liu, L. Ma, F. Hua, Z. Min, Y. Zhan, W. Zhang, et al., Exosomal circCARM1 from spheroids reprograms cell metabolism by regulating PFKFB2 in breast cancer, Oncogene 41 (14) (2022) 2012–2025.
[37] M.Z. Koh, W.Y. Ho, S.K. Yeap, N.M. Ali, C.Y. Yong, L. Boo, et al., Exosomal-microRNA transcriptome profiling of Parental and CSC-like MDA-MB-231 cells in response to cisplatin treatment, Pathol. Res. Pract. 233 (2022), 153854.
[38] F. Chen, J. Chen, L. Yang, J. Liu, X. Zhang, Y. Zhang, et al., Extracellular vesicle-packaged HIF-1alpha-stabilizing lncRNA from tumour-associated macrophages regulates aerobic glycolysis of breast cancer cells, Nat. Cell Biol. 21 (4) (2019) 498–510.
[39] Z.Z. Zhang, Z.Y. Shen, Y.Y. Shen, E.H. Zhao, M. Wang, C.J. Wang, et al., HOTAIR long noncoding RNA promotes gastric cancer metastasis through suppression of Poly r(C)-binding protein (PCBP) 1, Mol. Cancer Ther. 14 (5) (2015) 1162–1170.
[40] R. Sun, C. Qin, B. Jiang, S. Fang, X. Pan, L. Peng, et al., Down-regulation of MALAT1 inhibits cervical cancer cell invasion and metastasis by inhibition of epithelial-mesenchymal transition, Mol. Biosyst. 12 (3) (2016) 952–962.
[41] P. Ma, Y. Pan, W. Li, C. Sun, J. Liu, T. Xu, et al., Extracellular vesicles-mediated noncoding RNAs transfer in cancer, J. Hematol. Oncol. 10 (1) (2017) 57.
[42] H. Sontheimer, A role for glutamate in growth and invasion of primary brain tumors, J. Neurochem. 105 (2) (2008) 287–295.
[43] S. Koochekpour, S. Majumdar, G. Azabdaftari, K. Attwood, R. Scioneaux, D. Subramani, et al., Serum glutamate levels correlate with Gleason score and glutamate blockade decreases proliferation, migration, and invasion and induces apoptosis in prostate cancer cells, Clin. Cancer Res. 18 (21) (2012) 5888–5901.
[44] B.S. Taylor, M. Pal, J. Yu, B. Laxman, S. Kalyana-Sundaram, R. Zhao, et al., Humoral response profiling reveals pathways to prostate cancer progression, Mol. Cell Proteomics 7 (3) (2008) 600–611.
[45] Y.G. Chen, A.T. Satpathy, H.Y. Chang, Gene regulation in the immune system by long noncoding RNAs, Nat. Immunol. 18 (9) (2017) 962–972.
[46] L.B. Chipman, A.E. Pasquinelli, R.N.A. Targeting, Growing beyond the Seed, Trends Genet. 35 (3) (2019) 215–222.
[47] H.J. Wu, P.Y. Chu, Epigenetic regulation of breast cancer stem cells contributing to carcinogenesis and therapeutic implications, Int. J. Mol. Sci. 22 (15) (2021).
[48] S. Shukla, D. Penta, P. Mondal, S.M. Meeran, Epigenetics of breast cancer: clinical status of epi-drugs and phytochemicals, Adv. Exp. Med. Biol. 1152 (2019) 293–310.
[49] D.C. Temian, L.A. Pop, A.I. Irimie, I. Berindan-Neagoe, The epigenetics of triple-negative and basal-like breast cancer: current knowledge, J. Breast Cancer 21 (3) (2018) 233–243.
[50] A. Testa, E. Venturelli, M.F. Brizzi, Extracellular vesicles: new tools for early diagnosis of breast and genitourinary cancers, Int. J. Mol. Sci. 22 (16) (2021).
[51] D. Zhou, J. Gu, Y. Wang, H. Wu, W. Cheng, Q. Wang, et al., Long non-coding RNA NEAT1 transported by extracellular vesicles contributes to breast cancer development by sponging microRNA-141-3p and regulating KLF12, Cell Biosci. 11 (1) (2021) 68.